

The effect of composition gradients on deflagration-to-detonation transition in fuel-rich mixtures of H₂-air in an obstructed channel

Jumeng Fan, Huahua Xiao*

State Key Laboratory of Fire Science, University of Science and Technology of China
Hefei, Anhui, China

Abstract

Numerical simulations were performed to study the effect of composition gradients on detonation initiation in fuel-rich hydrogen-air mixtures in an obstructed channel with different obstacle arrangements. A third-order WENO method with adaptive mesh refinement (AMR) was used to solve the unsteady, fully-compressible reactive Navier-Stokes equations coupled to a calibrated chemical-diffusive model (CDM). The calibrated CDM can reproduce the major combustion wave properties in hydrogen-air mixtures over a wide range of equivalence ratios ϕ . The concentration gradient and obstacle arrangement effects for detonation initiation were examined in the mixture at an average H₂ concentration of 50 vol% in an obstructed channel with a blockage ratio of 0.3. It is discovered that the total heat release rate and speed of the leading reaction front have little difference for different transverse concentration gradients and obstacle arrangements before the transition to detonation. The occurrence distance to detonation initiation is shorter in the channel with unilateral obstacle arrangement than in the channel with bilateral obstacle arrangement, not correlating with concentration gradients. Detonation tends to be initiated near obstacles due to the frequent reflection and intersection of shock waves. More interestingly, for fuel-rich inhomogeneous hydrogen-air mixtures, detonation is more likely to be initiated in the high-concentration region. To provide a detailed analysis of detonation initiation, three idealized models were introduced to reproduce and understand detonation initiation caused by shock focusing and Mach-stem reflection. We conclude from the analysis that there are multiple ways detonation could be initiated in the obstructed channel, shock focusing and Mach-stem reflection at the flame front played a significant role in the detonation initiation by possibly creating a reactivity gradient. The results also show that the minimum shock strength required for detonation initiation decreases with the increase of the equivalence ratio for these three models. This is because ignition delay increases with the decrease of the equivalence ratio under the condition that the detonation is about to be ignited.

Keywords: Detonation initiation, Composition gradient, Composition gradient, Obstructed channel, Hydrogen-air mixture

1 Introduction

Understanding detonation initiation is important for detonation-based propulsion applications [1-4], astrophysical explosions [5-8], and safety in industries [6,9,10]. For example, a pulse detonation engine's successful operation requires fast and reliable detonation wave initiation by a reasonable amount of ignition energy. In a rotating detonation engine, detonation initiation in a pre-detonation tube is important for the stability of the detonation wave in the early stages. In astrophysics, thermonuclear deflagration can develop into a detonation in a supernova. This process could involve detonation initiation by a self-intensified unsteady flame. In industries, when detonation arises in unwanted explosions, which could occur in coal mines or fuel storage facilities, the destructive potential of explosions increases enormously. Therefore, it is important to understand the mechanism and predict the possibility of detonation initiation.

The large majority of previous studies were devoted to detonation initiation in uniform mixtures. Detonation can be initiated in different ways. The first route to initiating a detonation is direct initiation. When external energy added to a reactive mixture is enough at a timescale smaller than the acoustic time scale, detonation will be initiated [11]. In this way, detonation is sometimes initiated directly through shock focusing in an unburned region or boundary layer, without first producing a deflagration. Direct initiation of a detonation was first proposed by Lee [12,13]. The mechanism was then observed and demonstrated by experiments [12,14-16] and numerical simulations [17]. Another route is known as deflagration-to-detonation transition (DDT) [10], part of the response of a reactive gas to an intense localized explosion during deflagration. In the DDT process, detonation is sometimes initiated through a gradient of reactivity as a "hot spot" is produced by shock reflection [18,19], turbulent mixing [10], or boundary layer effects [20]. This mechanism was first proposed by Zeldovich et al. [21], and experimentally observed by Lee et al. [22]. The mechanism was then numerically demonstrated by Oran and Gamezo, as summarized in [10]. Shock focusing in an energetic gas can generate a detonation through processes that appear to be either direct initiation or hot spots. Detonation initiation through shock focusing is usually studied through a concave reflector [23] or focusing nozzle [24]. In addition, shock focusing and Mach-stem reflection caused by accelerating flame in obstacle channels can lead to a direct detonation initiation or DDT in an unburned mixture ahead of the flame front. For example, Goodwin et al. [17] showed that DDT may occur either through Mach-stem reflection or through direct initiation due to shock focusing. Similar experimental observations were also reported by Maeda et al. [14]. Details of detonation initiation by shock focusing at a flame front was reported in simulations [25], although the possibility of detonation initiation by other mechanisms in hydrogen-air mixtures with different equivalence ratio has not been explored.

In general, extensive knowledge is available for gaseous explosions in homogeneous reaction mixtures in this field. However, in real scenarios, detonation initiation usually occurs in non-uniform mixtures due to spatial gradients in fuels' concentration, floating effects, the limited time between ignition and fuel release, and the inhomogeneity of the combustible mixtures. Among the studies conducted in this field, Vollmer et al. [26] performed an experimental study of an obstacle-laden channel in which hydrogen was injected vertically and inhomogeneously. They discovered that in the non-uniform mixtures, the $L > 7\lambda$ criterion provided by Dorofeev et al. [27] was invalid. In this criterion, λ is the cell size of the detonation and L is the minimum space for detonation initiation. Also, Boeck et al. [28-31] investigated the effect of a concentration gradient in the hydrogen-air mixture on flame acceleration and the maximum measured pressure during detonation. They observed that in obstacle-laden channels, the concentration gradient, only in mixtures (with an average concentration less than 24 vol%), would promote flame acceleration and detonation initiation. For richer mixtures, the concentration gradient would reduce the flame acceleration and defer detonation initiation. However, in the smooth channel, flame acceleration in a non-uniform mixture is always greater than that in a uniform mixture. Also, the pressure measured in a non-uniform mixture is different from that in uniform mixtures. Thus, results based on uniform mixtures are not accurate for real scenarios. Wang

et al. [32] used a newly developed solver in the OpenFOAM CFD toolbox for mixtures with concentrated gradients. They found that in fuel-rich areas, hydrogen does not burn completely and this unburned hydrogen can be re-ignited by fresh air, which is significant in terms of accident safety. Karanam et al. [33,34] simulated the flame acceleration and DDT process in uniform and non-uniform hydrogen-air mixtures. By investigating the time scale analysis, they discovered that the chemical time scale of the hydrogen combustion mechanism was estimated at 10⁻⁶ to 10⁻⁴ s. Khodadadi et al. [35,36] using the OpenFOAM CFD toolbox solved the unsteady compressible Navier-Stokes equations and used the HLLC convective flux refraction method. They observed that for non-uniform mixtures, at blockage ratios of 30% and 60%, a higher blockage ratio caused faster flame acceleration and reduced the occurrence distance of detonation transition. Recently, DDT in non-uniform hydrogen-air mixtures in an obstructed channel was preliminary reported in simulations [37], the results show that DDT can be promoted by increasing the blockage ratio or placing obstacles along the sidewalls with lower H₂ concentration. These previous studies usually considered a single obstacle arrangement, i.e., obstacles uniformly placed either along both lower and upper sidewalls or only one sidewall of the channel. They, however, did not consider the influence of obstacle arrangement and composition gradient in inhomogeneous reaction mixtures.

As mentioned, studies performed on gas explosions for inhomogeneous reaction mixtures are sparse, it is essential to deeply understand the mechanism of detonation initiation and specify whether inhomogeneity of mixtures can increase the hazard of explosions. In the present article, numerical simulations were performed to study the effect of composition gradients on detonation initiation in fuel-rich hydrogen-air mixtures in an obstructed channel. The simulations solve the fully-compressible reactive Navier-Stokes equations coupled to a calibrated CDM [38] using a high-order numerical method on a dynamically adapting mesh. In addition, three idealized models were introduced to reproduce and understand detonation initiation caused by shock focusing and Mach-stem reflection, the idealized problems allow us to focus on the characteristics of detonation transition in mixtures with different concentration gradients.

2 Mathematical model

2.1 Governing equations

The numerical simulations solve the two-dimensional (2D), unsteady, fully-compressible reactive Navier-Stokes equations [37,39-41]:

$$\frac{\partial \rho}{\partial t} + \nabla \cdot (\rho \mathbf{U}) = 0, \quad (1)$$

$$\frac{\partial (\rho \mathbf{U})}{\partial t} + \nabla \cdot (\rho \mathbf{U} \mathbf{U}) + \nabla p = \nabla \cdot \hat{\tau}, \quad (2)$$

$$\frac{\partial (\rho E)}{\partial t} + \nabla \cdot ((\rho E + p) \mathbf{U}) = \nabla \cdot (\mathbf{U} \cdot \hat{\tau}) + \nabla \cdot (K \nabla T) - \rho q \dot{w}, \quad (3)$$

$$\frac{\partial (\rho Y)}{\partial t} + \nabla \cdot (\rho Y \mathbf{U}) + \nabla \cdot (\rho D \nabla Y) = \rho \dot{w}, \quad (4)$$

$$p = \rho RT/M, \quad (5)$$

where ρ is the density, t is the time, \mathbf{U} is the vector velocity, p is the pressure, $\hat{\tau}$ is the viscous stress tensor, E is the specific total energy, T is the temperature, \dot{w} is the chemical reaction rate, q is the chemical energy release, Y is the mass fraction of reactant, K is the thermal conductivity, D is the mass diffusivity, M is the molecular weight, and R is the universal gas constant. The viscous stress tensor is defined as

$$\hat{\tau} = \rho v \left((\nabla \mathbf{U}) - (\nabla \mathbf{U})^{T_r} - \frac{2}{3} (\nabla \cdot \mathbf{U}) \mathbf{I} \right), \quad (6)$$

where v is the kinematic viscosity, \mathbf{I} is the unit tensor, and the superscript T_r denotes matrix transposition. The specific total energy is calculated by

$$E = \frac{p}{(\gamma - 1)\rho} + \frac{1}{2} (\mathbf{U} \cdot \mathbf{U}), \quad (7)$$

where γ is the specific heat ratio which is taken as a constant.

The combustion of non-uniform hydrogen-air mixtures is modeled by a calibrated CDM. The reaction rate is defined as

$$\dot{w} \equiv dY/dt = -A\rho Y \exp(-E_a/RT), \quad (8)$$

where A and E_a are the pre-exponential factor and activation energy, respectively.

The kinematic viscosity, mass diffusivity, and thermal diffusivity are computed as $\mu = \mu_0 T^{0.7} / \rho$, $D = D_0 T^{0.7} / \rho$, and $K = k_0 T^{0.7} c_p / \rho$, respectively, where μ_0 , D_0 , and k_0 are the reference transport coefficients, $\mu_0 = D_0 = k_0$, and c_p is the specific heat at constant pressure. The CDM has been extensively tested and used in homogenous mixtures to solve a wide range of combustion problems [42], such as laminar [40,41] and turbulent flames [43], flame-shock interactions [25,41], DDT [10,13,19,25,37,44-46], and cellular detonations [47].

To extend the CDM to non-uniform hydrogen-air mixtures, the model is calibrated using an approach that combines the genetic algorithm and Nelder-Mead optimization scheme (GA-NM) based on a simplified Arrhenius type form of conversion of reactants to products (Eq. (8)). These optimal model parameters [48], A , E_a , q , and k_0 , were obtained through the GA-NM approach for hydrogen-air mixtures over a range of equivalence ratio from lower to upper flammability limit, i.e., $1.0 \leq \varphi \leq 7.14$. The ratio of specific heats $\gamma = 1.21$ and the molecular weight of the mixture $M = 0.025$ kg/mol are set as constants over the entire domain. The calibrated CDM can well reproduce the intended combustion wave properties including laminar flame speed S_L , laminar flame thickness x_L , adiabatic flame temperature T_b , and equilibrium flame temperature T_{cv} , half-reaction thickness x_d . It has been used to simulate the flame acceleration and detonation transition in inhomogeneous mixtures [48] and the results are in good agreement with experiments.

2.2 Numerical method and details

Fig. 1 shows the two-dimensional computational domain. It is an obstructed channel, 5.4 m (L) \times 0.06 m (H). This study considers two different obstacle arrangements: (a) Bilateral, obstacles are placed at both the lower and upper sidewalls, (b) unilateral, obstacles are placed at only the lower sidewall of the channel. The spacing between neighboring obstacles is $S = 0.3$ m, and the blockage ratio is $BR = 30\%$. Fig. 2 shows four different linear hydrogen concentration (Y_{H_2}) gradients along the transverse direction in four inhomogeneous cases studied in this article. Table 1 describes details of the four cases, including obstacle arrangement, and the H₂ concentration at the lower wall, upper wall, and central axis. The average H₂ concentration in the computational domain of these gradients is all 50 vol%. Therefore, the overall reactivity and exothermicity in terms of concentration are held fixed, and this allows direct comparisons between different concentration gradients.

The governing equations are solved using a third-order WENO algorithm with HLLC fluxes. The time integration is advanced using a second-order explicit Runge-Kutta scheme [49]. The grid in the computational domain is dynamically refined using AMR [50]. The AMR helps resolve important flow features, such as flames, shocks, and chemical structures. No-slip and adiabatic boundary conditions are used at the channel walls and obstacle surfaces. The flame was ignited using a semi-circular region of hot, burned material at 101325 Pa centered on the channel axis at the left end.

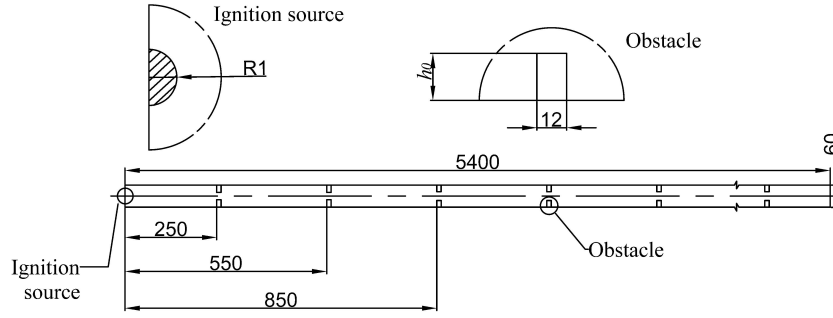


Figure 1: Computational domain of a closed and obstructed channel with a blockage ratio of 30%, referring to the experiment by Boeck et al. [51]. Unit is in mm.

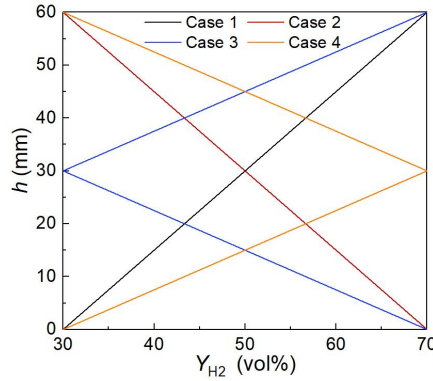


Figure 2: Hydrogen concentration gradients (Y_{H_2}) along the transversal direction.

Table 1: Details of the four inhomogeneous cases studied in this article.

Case	Obstacle arrangement	Lower wall Y_{H_2} (vol%)	Central axis Y_{H_2} (vol%)	Upper wall Y_{H_2} (vol%)
1	Bilateral	30	70	30
2	Bilateral	70	30	70
3	Unilateral	70	50	30
4	Unilateral	30	50	70

2.3 Grid resolution test and comparison to experiment

Grid resolution tests were performed by varying the minimum cell size dx_{\min} at the most refined level of the computational mesh for the case of stoichiometric hydrogen-air mixture. Fig. 3a shows the variation of the speed of leading tip of reaction front as a function of flame tip for different minimum grid sizes $dx_{\min} = 1/80$ cm (125 μ m), $1/160$ cm (62.5 μ m), $1/320$ cm (31.3 μ m), and $1/640$ cm (15.6 μ m). It shows that all the four grid resolutions give reasonable results and the FA and DDT is converged at the grid with $dx_{\min} = 1/320$ cm, corresponding to 11 computational cells in the flame and 6 cells in half-reaction thickness for $\varphi = 1$. Tests were also conducted with different maximum grid sizes, $dx_{\max} = 4, 2, 1,$ and 0.5 mm at the coarsest level, as shown in Fig. 3b. It was found $dx_{\max} = 2$ mm is adequate for computing DDT. We used $dx_{\min} = 1/320$ cm and $dx_{\max} = 2$ mm for the computations. Previous work by Gamezo et al. [18] and Xiao et al. [37,46] also shows that this grid resolution is adequate for CDM to calculate the FA and DDT in hydrogen-air mixture.

Fig. 4 compares the computed and measured [51] speed of the leading tip as a function of reaction front position for (a) homogeneous mixture with H₂ concentration 25 vol%, (b) inhomogeneous mixture at an average H₂ concentration 25 vol%, (c) homogeneous mixture with H₂ concentration 30 vol%, and (d) inhomogeneous mixture at an average H₂ concentration 30 vol%. Overall, the numerical results are in good agreement with the experiments.

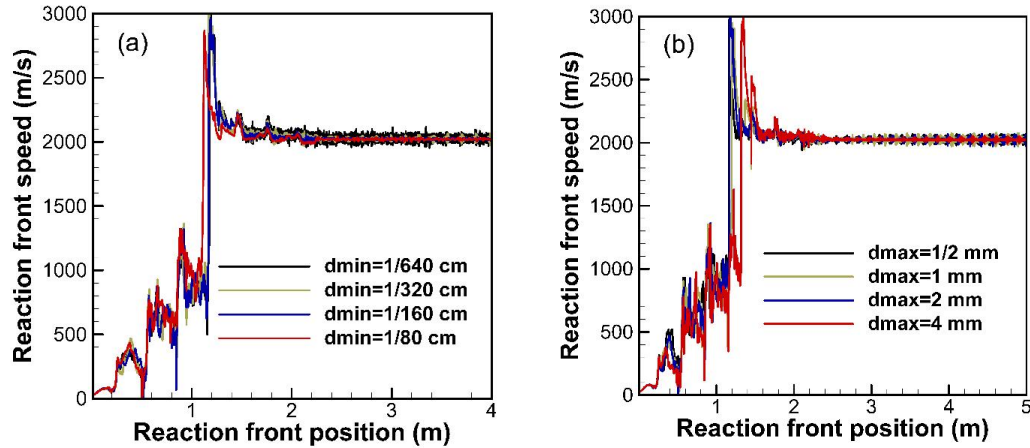


Figure 3: Variation of the leading tip of reaction front at different values of (a) minimum grid size dx_{\min} and (b) maximum grid size dx_{\max} .

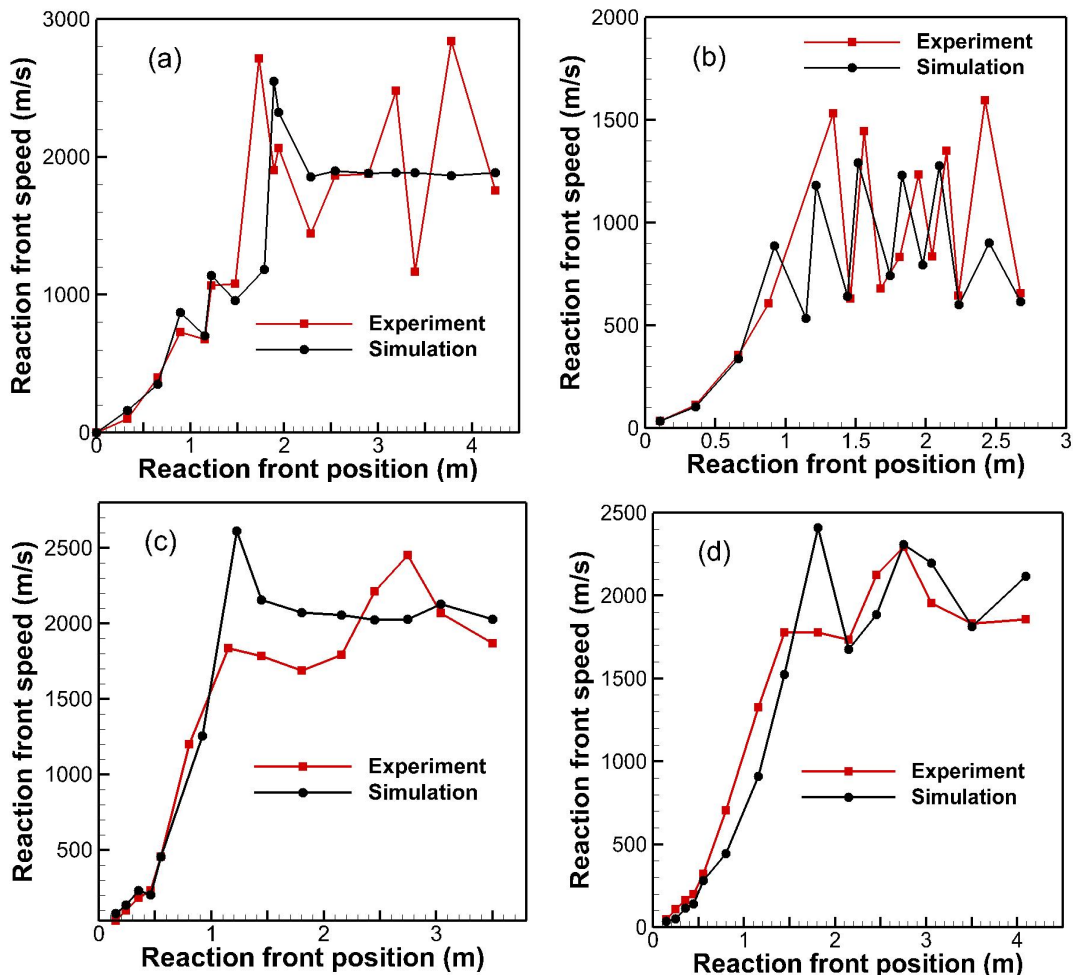


Figure 4: Computed and measured speed [51] of the leading edge of reaction front as a function of its position in (a) homogeneous mixture with H₂ concentration 25 vol%, (b) inhomogeneous mixture at an average H₂ concentration 25 vol%, (c) homogeneous mixture with H₂ concentration 30 vol%, and (d) inhomogeneous mixture at an average H₂ concentration 30 vol%.

3 Results and discussion

3.1 Flame propagation and detonation initiation

Fig. 5 shows a time sequence of selected temperature fields of flame acceleration and detonation initiation for a 50 vol% uniform hydrogen-air mixture in a channel ($BR = 30\%$) with bilateral and unilateral obstacle arrangements. From these, we note the flame acceleration and shock formation, and see when and where DDT occurred. The early flame acceleration in the channel primarily results from the thermal expansion of hot combustion products [39,52,53] and flame-vortex interactions [54]. As the flame continues to accelerate, compression waves are produced and converge into a shock wave in the front of the flame, as shown in Fig. 5a at 15.5 ms and Fig. 5b at 11.31 ms. The significant compression of unburned gas by shock waves contributes to the increase in the heat release rate. The interactions of the flame and shocks cause more flame instabilities, e.g., Rayleigh-Taylor and Richtmyer-Meshkov instabilities [40,41,52]. These effects further accelerate flame and flow, and thus generate a stronger leading shock wave downstream of the flame front.

In the channel with bilateral obstacle arrangement, the leading shock reflects from every obstacle pair, producing two reflected shocks (marked as RS1, 2), as shown in Fig. 5a at 15.59 ms. The two reflected shocks crisscross each other and form a Mach stem (marked as MS1), as shown in Fig. 5a at 15.63 ms. After passing through the obstacles, RS1 and RS2 are reflected by the lower and upper sidewalls respectively, and form two Mach stem (marked as MS2, 3), as shown in Fig. 5a at 15.72 ms. The flame front collides with the Mach stem MS1 and creates a small hot spot (marked as HS1) in Fig. 5a at 15.72 ms. Then, a detonation (marked as D1) is initiated by Zeldovich's reactivity-gradient mechanism, as shown in Fig. 5a at 15.76 ms. In the channel with unilateral obstacle arrangement, the leading shock reflects from every obstacle, producing a reflected shock (marked as RS3), as shown in Fig. 5b at 12.46 ms. RS3 continues to reflect by the sidewalls and forms the Mach stems (marked as MS4, 5), as shown in Fig. 5b at 12.97 ms and 13.52 ms. The flame front collides with the Mach stem MS4 and creates a small hot spot (marked as HS2) in Fig. 5b at 13.52 ms. Then, a detonation (marked as D2) is initiated by Zeldovich's reactivity-gradient mechanism, as shown in Fig. 5a at 13.53 ms. In the cases with the other obstacle arrangements and composition gradients, DDT also often occurs in the area near Mach stems due to shock-flame, shock-shock, or shock-obstacle interactions. And the detonation wave soon travels quickly through the unburned mixture.

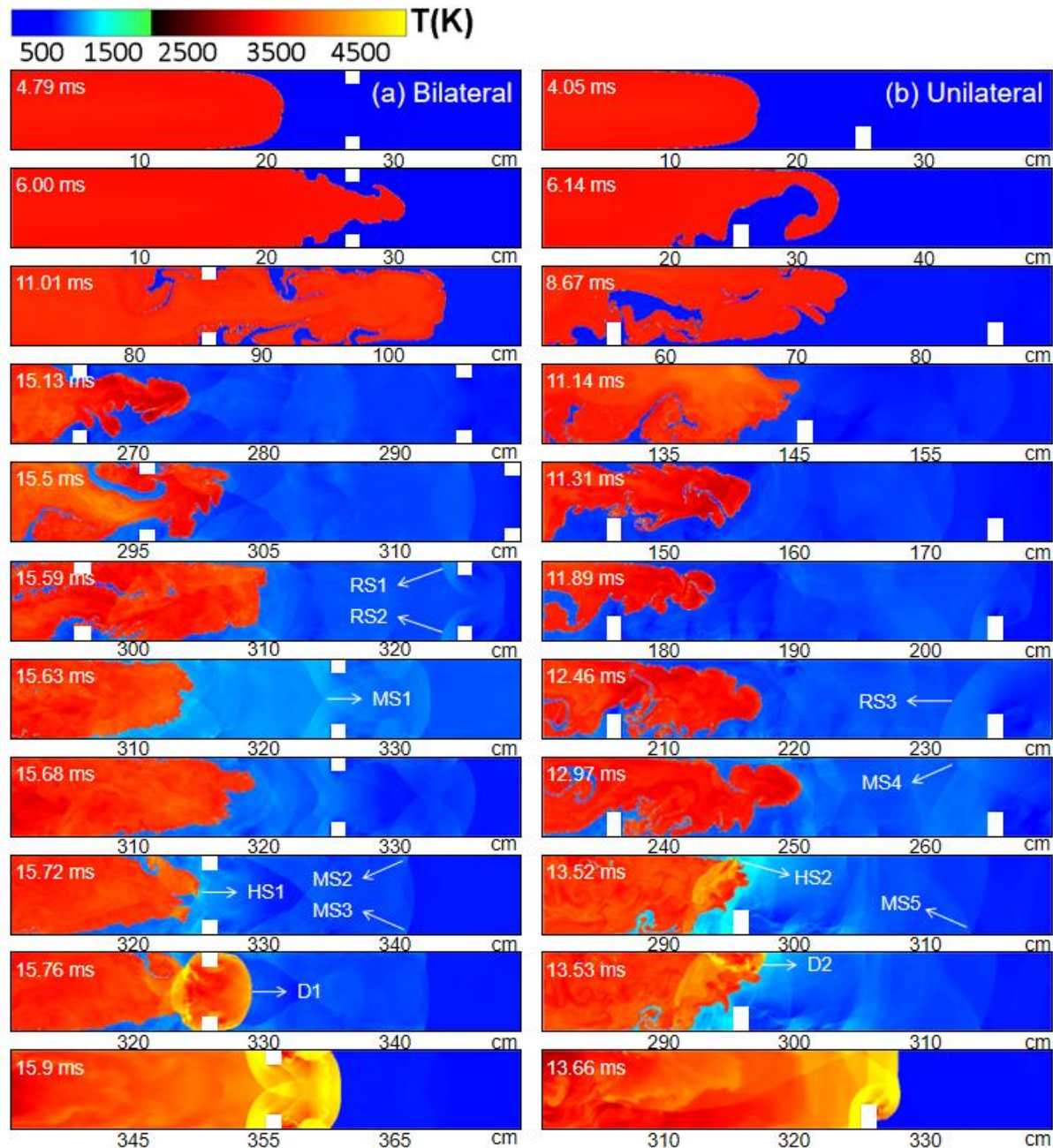


Figure 5: Numerical temperature fields for 50 vol% uniform hydrogen-air mixture in the channel with (a) bilateral obstacle arrangement and (b) unilateral obstacle arrangement. RS: reflected shock; MS: Mach stem; HS: hot spot; D: detonation.

Fig. 6 compares the reaction front surface area, total heat release rate, and speed of the leading reaction front as a function of time for a 50 vol% uniform hydrogen-air mixture in a channel with bilateral and unilateral obstacle arrangement. Fig. 6a shows that the reaction front in the channel with unilateral obstacle arrangement has a significantly larger reaction-front surface area and the maximum surface area occurs at an earlier time than that in the channel with bilateral obstacle arrangement. Once the detonation is initiated, the flame surface area sharply decreases with the fast depletion of the fuel and oxidizer. The total heat release rate is higher in the channel with obstacles placed at the lower sidewall throughout the entire process due to the larger reaction front area, as shown in Fig. 6b.

Correspondingly, the speed of the leading reaction front is faster and the occurrence distance of DDT is shorter, as shown in Fig. 6c.

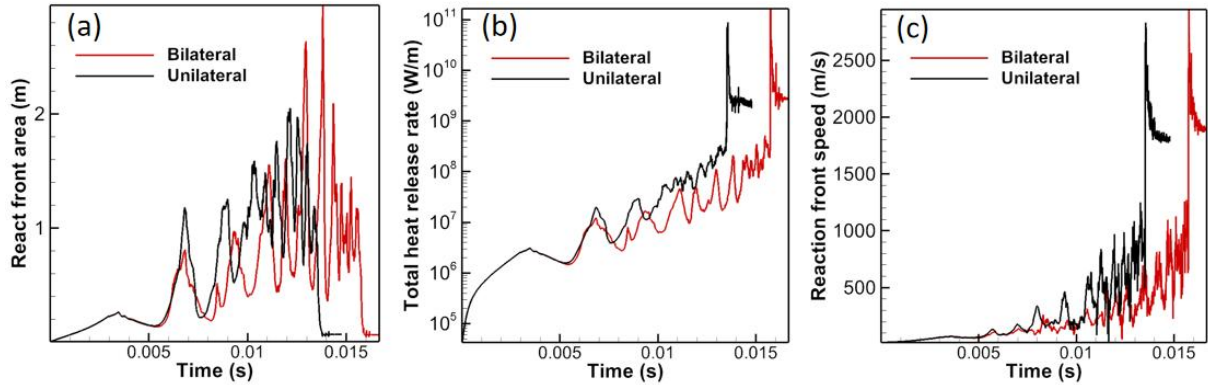


Figure 6: Comparison of (a) reaction front surface area, (b) total heat release rate, and (c) speed of the leading reaction front as a function of time for 50 vol% uniform hydrogen-air mixture in a channel with bilateral and unilateral obstacle arrangement.

3.2 Effect of composition gradient on detonation initiation

Fig. 7 compares the speed of the leading reaction front and total heat release rate as a function of the reaction front position for the four cases described in Table 1. The blockage ratio, the distance between obstacles, and the average concentration are all the same in the four cases. Therefore, when the flame passes the same distance, it consumes the same amount of mixture. As shown in Fig. 7, before the transition to detonation, the total heat release rate as a function of the reaction front position has little difference in different cases for mixtures with different transverse concentration gradients, which leads to almost the same speed of the leading reaction front. In addition, it is also observed that the occurrence distance to detonation transition in the channel with the same obstacle arrangement is not affected by the concentration gradient. Detonation initiated occurred near the twelfth obstacle in the channel with obstacles placed at both the lower and upper sidewalls, near the tenth obstacle in the channel with obstacles placed at the lower sidewall.

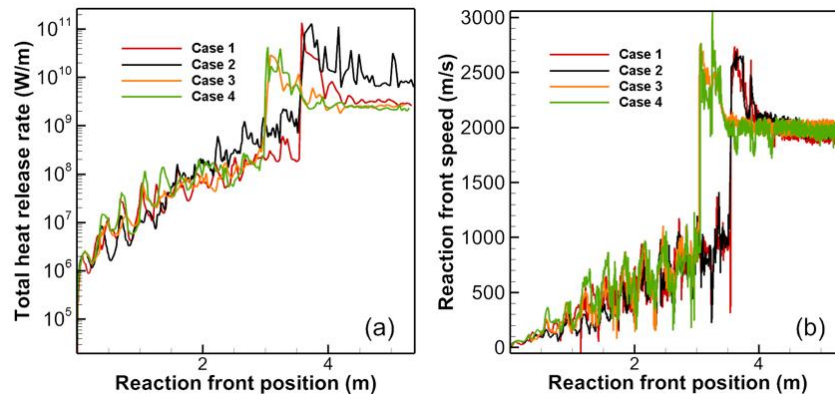


Figure 7: Comparison of (a) total heat release rate and (b) speed of the leading reaction front as a function of position for the four cases described in Table 1.

Fig. 8 shows detailed temperature fields of the detonation initiation for the four cases described in Table 1. In case 1, two reflected shocks cross each other and form a Mach stem (marked as MS1), the interaction between MS1 and flame causes DDT. In case 2, the leading shock interacts with the side walls to form two Mach stems (marked as MS2 and MS3), MS2 and MS3 then collide with the obstacles and directly cause detonations (marked as D2 and D3). In cases 3 and 4, the shock wave diffracted from the obstacle and interacted with the side walls, forming two Mach stems (marked as

MS4 and MS5). The collision between Mach stems and flame causes DDT. In these four cases, detonation initiation tends to occur near obstacles. This is because the frequent reflection and intersection of shock waves can easily lead to the formation of Mach stems, triggering detonation initiation. In addition, detonation initiation is more likely to occur in the high-concentration region.

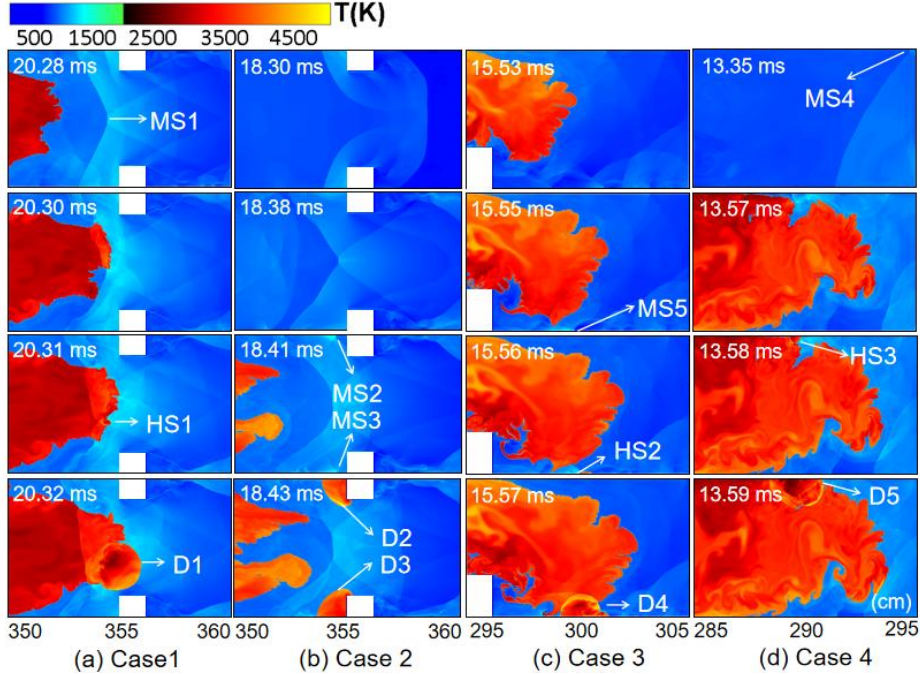


Figure 8: Numerical temperature fields of the detonation initiation process for the four cases described in Table 1. MS: Mach stem; HS: hot spot; D: detonation.

3.3 Idealized models of detonation initiation

The intricate interactions of the reaction waves and flow fields in Fig. 8 pose complications to the in-depth analysis of the detonation initiation. As shown in Fig. 9, we have now formulated and examined three idealized problems that are used to give us insights into essential physics. In these three models, gases are quiescent at the initial condition, dark blue area and red area represent unburned mixture and burned mixture, respectively. The physical conditions are set to correspond approximately to the state variables of the unburned and burned gases around the focusing spot (see Fig. 8) before the shocks reached it in the prior calculation of the obstructed channel. The temperatures in the unburned and burned regions are 446 and 2500 K, respectively, and the pressure is 7.5 atm. The mesh refinement is dynamically adapted to follow the important flow features, such as reaction fronts, shocks, and shear flows. The cell size on the base grid is $d_{max} = 200 \mu\text{m}$. The minimum cell size is $d_{min} = 6.25 \mu\text{m}$, approximately corresponding to 31 and 56 grid points per laminar flame thickness and half-reaction thickness, respectively.

The idealized model a in Fig. 9a simplifies the mechanism of detonation initiation in Fig. 8a. Non-reflecting boundary conditions are used at all four boundaries. Two incident normal shock waves (marked as IS1 and IS2 in Fig. 9a at $0.0 \mu\text{s}$) with the same Mach number are symmetrically imposed in the burned gas near the left and right boundaries. The state variables behind these two shocks are set to be properties of a normal shock propagating at a given Mach number into burned gas. As the shocks start to move in opposite directions toward the center of the domain, secondary shocks propagate into the unburned gas on the left and right sides, as shown in Fig. 9a at $2.478 \mu\text{s}$. The result of the interaction of the shock with the interface is a transmitted shock and a reflected shock formed in each of the left and right parts of the domain, as shown in Fig. 9a at $4.497 \mu\text{s}$. These two transmitted shocks then become inclined due to drag at the interface. The idealized model ensures that the two incident

shocks and the two transmitted shocks collide right at the flame front at the center of the domain without disturbing it before focusing. If the incident shock waves are strong enough, a detonation (marked as D1 in Fig. 9a at 5.377 μ s) will be initiated directly at the focusing location almost immediately after the shock collision.

The idealized model b in Fig. 9b simplifies the mechanism of detonation initiation in Fig. 6b. Non-reflecting boundary conditions are used for the left and right boundaries, and No-slip and adiabatic boundary conditions are used for the upper and lower boundaries. A pair of obstacles are placed on the upper and lower walls. An arc-shaped incident shock wave (marked as IS3 in Fig. 9b at 0.0 μ s) is imposed near the left boundary. The state variables behind the arc-shaped incident are set to be properties of a normal shock propagating at a given Mach number into unburned gas. The shock starts to move to the right and forms Mach stems on the upper and lower walls (marked as MS1 and MS2 in Fig. 9b at 3.878 μ s). If the incident shock wave is strong enough, two detonations (marked as D2 and D3 in Fig. 9b at 4.690 μ s) will be initiated directly at the collision location almost immediately after the Mach stems collision with the obstacles.

The idealized model c in Fig. 9c simplifies the mechanism of detonation initiation in Fig. 8c and 8d. Non-reflecting boundary conditions are used for the left and right boundaries, and No-slip and adiabatic boundary conditions are used for the upper and lower boundaries. An arc-shaped incident shock wave (marked as IS4 in Fig. 9c at 0.0 μ s) is imposed near the left boundary. The state variables behind the arc-shaped incident are set to be properties of a normal shock propagating at a given Mach number into unburned gas. The shock starts to move right and lead to two Mach stems on the upper and lower walls (marked as MS3 and MS4 in Fig. 9c at 3.019 μ s). The Mach stems enhance during the forward movement and lead to two hot spots (marked as HS1 and HS2 in Fig. 9c at 4.036 μ s), and DDT occurred due to Zeldovich's reactivity-gradient mechanism in Fig. 9c at 4.486 μ s.

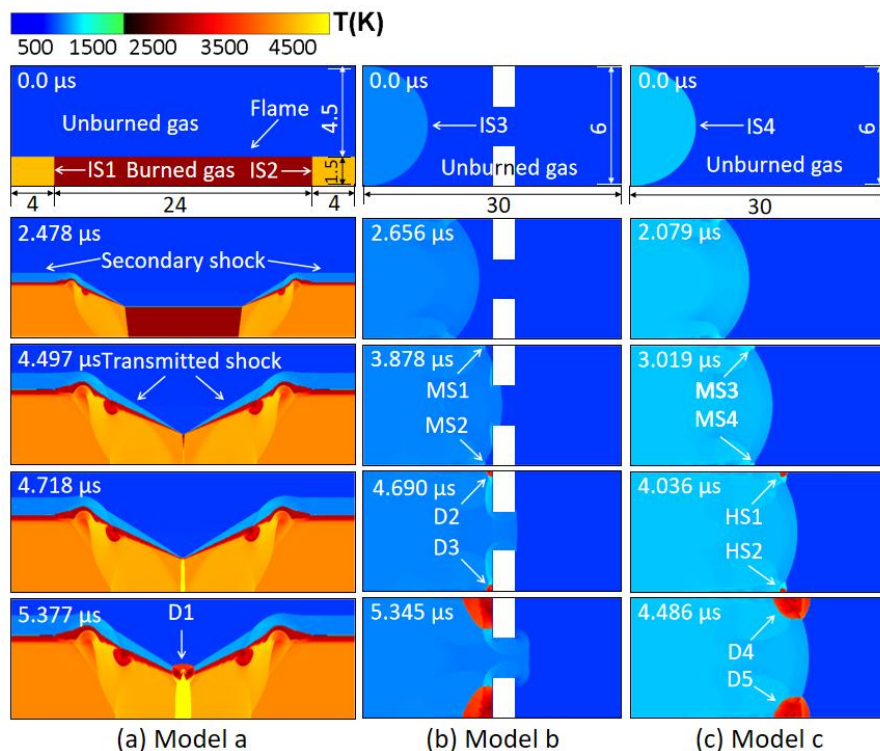


Figure 9: Temperature fields showing three idealized models of detonation initiation. The unit of length is in mm. IS: incident shock; MS: Mach stem; HS: hot spot; D: detonation.

When the shock waves in the three ideal models are strong enough, detonation will be ignited in the computational domain. Fig. 10 shows the minimum Mach number of shock waves required for

detonation initiation in the three idealized models at different equivalence ratios of hydrogen-air mixtures. The results show that the minimum Mach number required for detonation initiation decreases with the increase of the equivalence ratio for these three models.

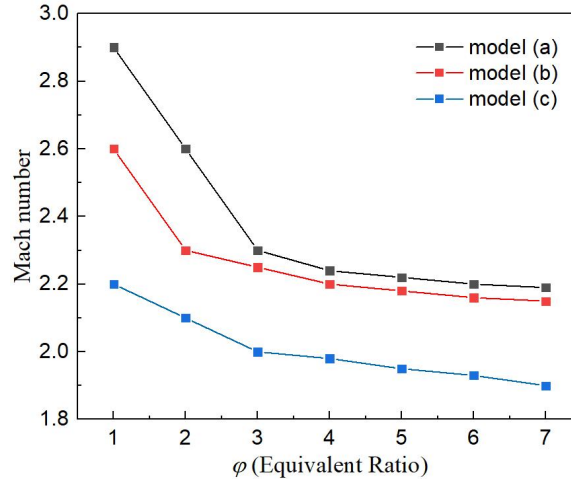
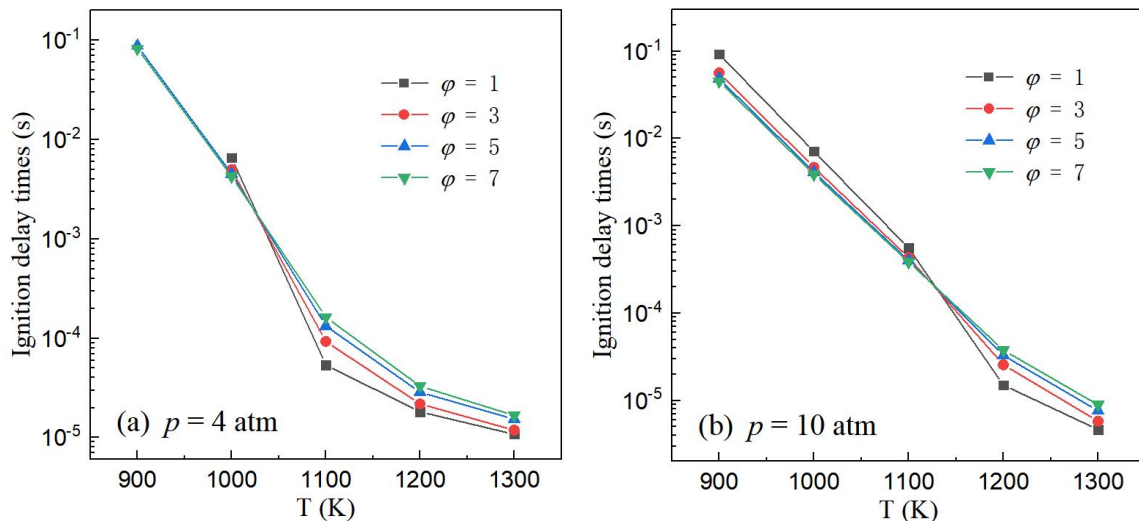


Figure 10: The minimum Mach number of shock wave required for detonation of the three idealized models at different equivalence ratios of hydrogen-air mixtures.

3.4 Ignition delay and sensitivity analysis

Fig. 11 gives the ignition delays of the hydrogen-air mixture with different equivalence ratios at pressures of 4 atm, 10 atm, 30 atm, and 50 atm. Results show that an obvious influence of equivalence ratio on the ignition of syngas mixtures is presented under fuel-rich conditions. As shown in Fig. 11a under the condition of 4 atm, at low temperatures ($T < 1000$ K), ignition delay increases with the decrease of the equivalence ratio; At high temperatures ($T > 1000$ K), the influence of the equivalence ratio on ignition delay demonstrates an opposite trend to that at low temperatures, ignition delays increase with the of increase equivalence ratio. This opposite influence of equivalence ratio on ignition delay at low and high temperatures certainly brings a cross-over point. It is noted that the cross-over point shifts to the higher temperature at higher pressure. Under the condition that the detonation is about to be ignited, i.e., 900 K and 50 atm, ignition delay increases with the decrease of the equivalence ratio. This verifies why the minimum shock intensity required for detonation initiation decreases with the increase of the equivalence ratio for these three models.



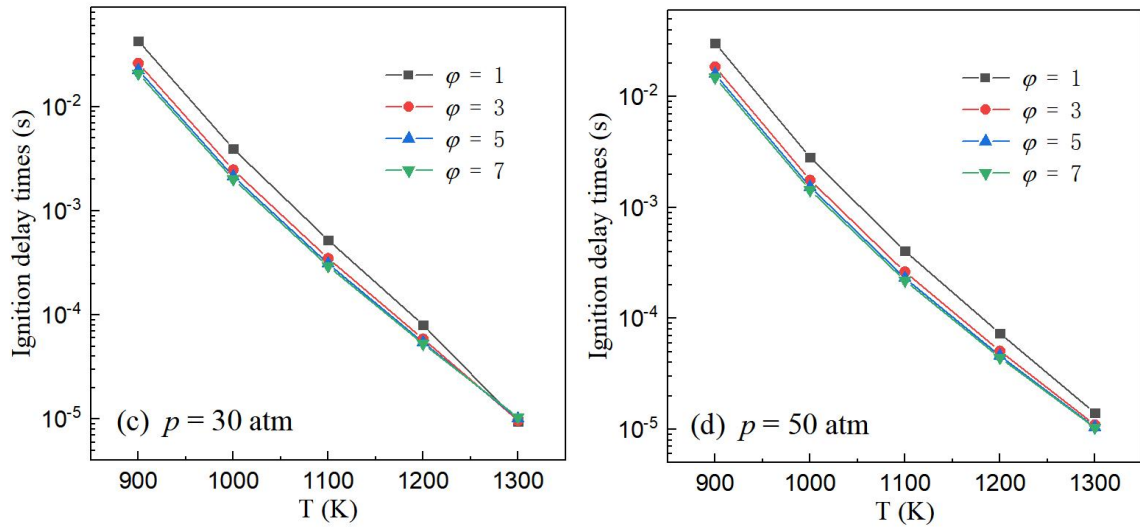


Figure 11. Ignition delays of uniform hydrogen-air mixtures at different equivalence ratios and pressures. (a) $p = 4$ atm; (b) $p = 10$ atm; (c) $p = 30$ atm; (d) $p = 50$ atm.

To identify the dominant elementary reactions in the ignition process of syngas mixtures and interpret the chemical kinetic effect of equivalence ratio on ignition chemistry, the bruteforce sensitivity analysis was made at pressures of 4 atm, 10 atm, 30 atm, and 50 atm. Fig. 12 gives the sensitivity analysis at the temperature of 1100 K. The rate constant of i th reaction k_i is individually multiplied and divided by a factor of 2 and 0.5, and the ignition delays $\tau(2k_i)$ and $\tau(0.5k_i)$ are calculated with the reaction rates of $2k_i$ and $0.5k_i$, respectively. The normalized sensitivity coefficient of the i th reaction is defined as

$$S = \frac{\tau(2k_i) - \tau(0.5k_i)}{1.5\tau(k_i)}, \quad (14)$$

where k_i is the rate constant of i th reaction, and S is the ignition delay time. A negative value of the sensitivity coefficient indicates a promoting effect on the ignition, and vice versa.

A strong influence of the equivalence ratio on ignition delay was observed through the sensitivity analysis. Under the lower-pressures condition of 4 atm, the ignition delay is most sensitive to the reaction $\text{H} + \text{O}_2 = \text{O} + \text{OH}$ (R1). The promoting role of reaction R1 is decayed with the increase of the equivalence ratio of the reaction mixture, leading to the faster ignition of mixtures with lower equivalence. With an increase of pressure, the sensitivity coefficient of hydrogen-mixture is increased for reaction $\text{H}_2\text{O}_2 + \text{H} = \text{HO}_2 + \text{H}_2$ (R24) and decreased for reaction R1 with the increase of equivalence ratio. The promoting role of R1 becomes non-dominant in the ignition kinetic compared to that of reaction R24. The promoting role of reaction R24 is decayed with the decrease of the equivalence ratio of the reaction mixture, resulting in increased ignition delay of the mixture with a higher equivalence ratio.

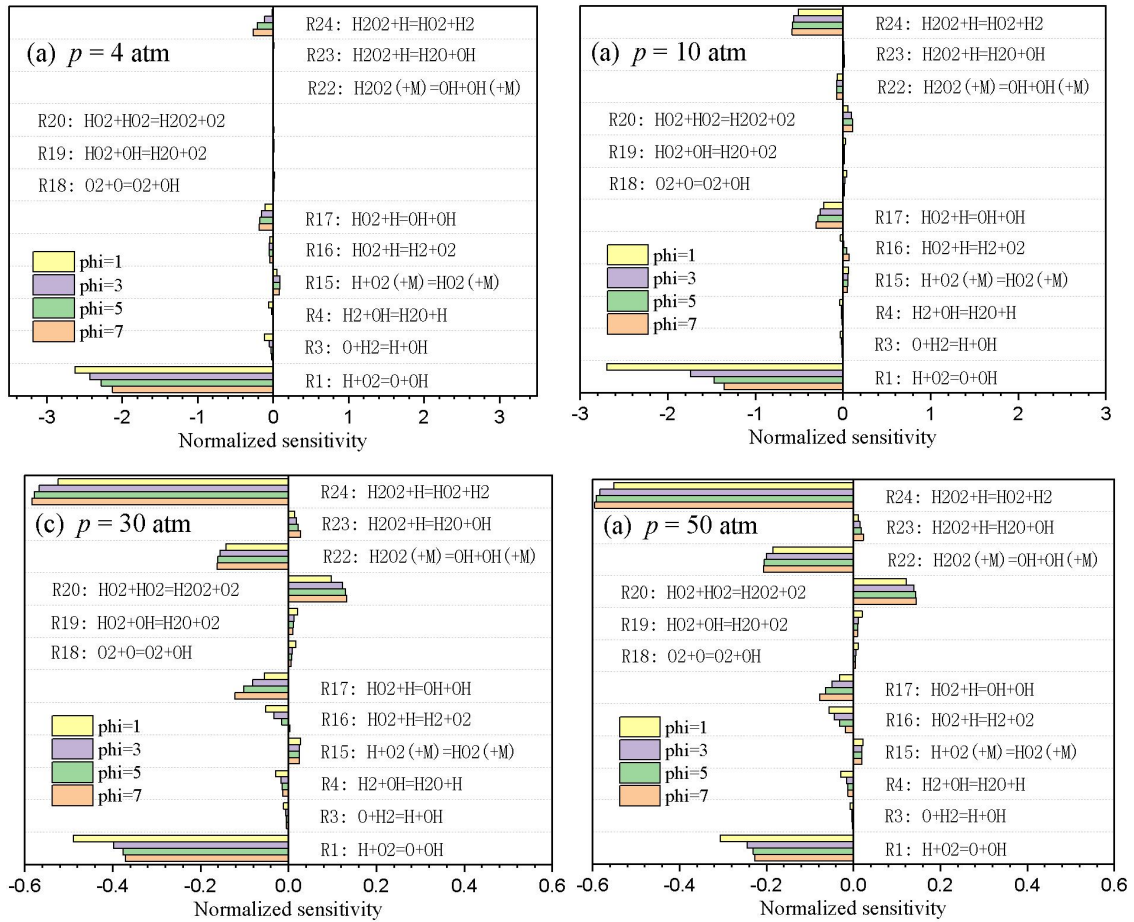


Figure 12: Sensitivity analysis of uniform hydrogen-air mixtures at $T = 1100$ K and different pressures. (a) $p = 4$ atm; (b) $p = 10$ atm; (c) $p = 30$ atm; (d) $p = 50$ atm.

3 Results and discussion

Numerical simulations were performed to study the effect of composition gradients on detonation initiation in fuel-rich hydrogen-air mixtures in an obstructed channel with different obstacle arrangements. A third-order WENO method with AMR was used to solve the unsteady, fully-compressible reactive Navier-Stokes equations coupled to a calibrated CDM. The calibrated CDM can reproduce the major combustion wave properties in hydrogen-air mixtures over a wide range of equivalence ratios ϕ . The simulated flame acceleration and detonation transition are in good agreement with previous experiments [48]. Different obstacle arrangements, i.e., bilateral and unilateral obstacle arrangements, all with the same blockage ratio of 0.3, were used to examine the effect of composition gradients on detonation initiation in fuel-rich hydrogen-air mixtures at an average H₂ concentration of 50 vol% in an obstructed channel.

In general, the simulations show that as the flame passes over obstacles, flame acceleration is strongly influenced by the flow in the obstacle wakes through the processes of flame-vortex interactions and flame stretching. By contrast, shock-shock and flame-shock interactions dominate the flame acceleration in the later stages by producing strong flame instabilities such as Richtmyer-Meshkov instabilities and highly corrugated flames. Detonation is also often initiated in the area near Mach stems formed by the interaction of shocks with obstacles or walls.

Influences of the concentration gradient and obstacle arrangement were examined for detonation initiation in the mixture at an average H₂ concentration of 50 vol%. It is discovered that before the transition to detonation, the total heat release rate as a function of the reaction front position has little difference for different transverse concentration gradients and obstacle arrangements, which leads to almost the same speed of the leading reaction front. The occurrence distance to detonation initiation is shorter in the channel with unilateral obstacle arrangement than in the channel with bilateral obstacle arrangement, not correlating with concentration gradients. Detonation tends to be initiated near obstacles due to the frequent reflection and intersection of shock waves. In addition, for fuel-rich inhomogeneous hydrogen-air mixtures, detonation is more likely to be initiated in the high-concentration region, i.e., in the 70 vol% hydrogen-air mixture.

Three idealized models were introduced to reproduce and understand detonation initiation caused by shock focusing and Mach-stem reflection. We conclude from the analysis that there are multiple ways detonation could be initiated in the obstructed channel, shock focusing and Mach-stem reflection at the flame front played a significant role in the detonation initiation by possibly creating a reactivity gradient. In the first model, two incident normal shock waves were symmetrically imposed in the flame on the two sides of the computational domain. These two shocks move in opposite directions and collide at the flame front, igniting a detonation. In the second model, an arc-shaped incident shock wave is imposed near the left boundary. The shock starts to move to the right and forms Mach stems on the upper and lower walls. Mach stems collide with the obstacles and ignite detonations. In the third model. The Mach stems formed on the upper and lower walls are enhanced during the forward movement and lead to hot spots and gradually develop into a detonation. To examine the effect of shock strength on detonation initiation, incident shock waves with different Mach numbers were considered. The results also show that the minimum shock strength required for detonation initiation decreases with the increase of the equivalence ratio for these three models. This is because ignition delay increases with the decrease of the equivalence ratio under the condition that the detonation is about to be ignited.

The ignition delay time was calculated using the detailed chemical reaction model of Chemkin to further confirm the effect of the equivalence ratio on the detonation initiation. Results show that an obvious influence of equivalence ratio on the ignition of syngas mixtures is presented under fuel-rich conditions. At low temperatures, ignition delays increase with the decrease of the equivalence ratio; At high temperatures, the influence of the equivalence ratio on ignition delay demonstrates an opposite trend to that at low temperatures, ignition delays increase with the of increase equivalence ratio. This opposite influence of the equivalence ratio on ignition delay at low and high temperatures certainly brings a cross-over point. It is noted that the cross-over point shifts to the higher temperature at higher pressure. Under the condition that the detonation is about to be ignited, i.e., 900 K and 50 atm, ignition delay increases with the decrease of the equivalence ratio. This further verifies why the minimum shock intensity required for detonation initiation decreases with the increase of the equivalence ratio for these three models. Through sensitivity analysis, it is found that with the increase of pressure, the ignition delay is most sensitive to the reaction $\text{H}_2\text{O}_2 + \text{H} = \text{HO}_2 + \text{H}_2$ (R24). In addition, the promoting role of reaction R24 decreases with the reduction of the equivalence ratio of the reaction mixture, increasing the ignition delay of the mixture with a high equivalence ratio.

The results of this study can be helpful to the development of safety in industries, e.g., fuel storage facilities, power plants, chemical plants, and explosion attenuators. Further work remains to be conducted to extend the study to fuel-lean mixtures and explore the effect of channel size, obstacle spacing, and fuel nonequidiffusivity.

References

- [1] Xia ZJ, Luan MY, Liu XY, Wang JP. (2020). Numerical simulation of wave mode transition in rotating detonation engine with OpenFOAM. *Int J Hydrogen Energy*. 45: 19989-19995.

- [2] Liu XY, Luan MY, Chen YL, Wang JP. (2020). Flow-field analysis and pressure gain estimation of a rotating detonation engine with banded distribution of reactants. *Int J Hydrogen Energy*. 45: 19976-19988.
- [3] Jiang H, Huang Y. (2022). Numerical investigation of non-premixed H₂-Air rotating detonation combustor with different equivalence ratios. *Journal of Physics: Conference Series*. 2235: 012011 (5 pp.)-012011 (5 pp.).
- [4] Elhawary S, Saat A, Wahid MA, Ghazali AD. (2020). Experimental study of using biogas in pulse detonation engine with hydrogen enrichment. *Int J Hydrogen Energy*. 45: 15414-15424.
- [5] Brooker E, Plewa T, Fenn D. (2021). Type Ia supernovae deflagration-to-detonation transition explosions powered by the Zel'dovich reactivity gradient mechanism. *Mon Not R Astron Soc*. 501: L23-L27.
- [6] Oran ES. (2015). Understanding explosions - From catastrophic accidents to creation of the universe. *Proceedings of the Combustion Institute*. 35: 1-35.
- [7] Oran ES. (2005). Astrophysical combustion. *Proceedings of the Combustion Institute*. 30: 1823-1840.
- [8] Gamezo VN, Khokhlov AM, Oran ES, Chtchelkanova AY, Rosenberg RO. (2003). Thermonuclear supernovae: Simulations of the deflagration stage and their implications. *Science*. 299: 77-81.
- [9] Zhang X, Yu J, Huang T, Jiang G, Zhong X, Saeed M. (2019). An improved method for hydrogen deflagration to detonation transition prediction under severe accidents in nuclear power plants. *Int J Hydrogen Energy*. 44: 11233-11239.
- [10] Oran ES, Gamezo VN. (2007). Origins of the deflagration-to-detonation transition in gas-phase combustion. *Combust Flame*. 148: 4-47.
- [11] Kiverin AD, Kassoy DR, Ivanov MF, Liberman MA. (2013). Mechanisms of ignition by transient energy deposition: Regimes of combustion wave propagation. *Physical Review E*. 87.
- [12] Lee JHS, Higgins AJ. (1999). Comments on criteria for direct initiation of detonation. *Philosophical Transactions of the Royal Society a-Mathematical Physical and Engineering Sciences*. 357: 3503-3521.
- [13] Zipf RK, Jr., Gamezo VN, Mohamed KM, Oran ES, Kessler DA. (2014). Deflagration-to-detonation transition in natural gas-air mixtures. *Combust Flame*. 161: 2165-2176.
- [14] Maeda S, Minami S, Okamoto D, Obara T. (2016). Visualization of deflagration-to-detonation transitions in a channel with repeated obstacles using a hydrogen-oxygen mixture. *Shock Waves*. 26: 573-586.
- [15] Zipf RK, Jr., Gamezo VN, Sapko MJ, Marchewka WP, Mohamed KM, Oran ES, Kessler DA, Weiss ES, Addis JD, Karnack FA, Sellers DD. (2013). Methane-air detonation experiments at NIOSH Lake Lynn Laboratory. *J Loss Prev Process Indust*. 26: 295-301.
- [16] Zhang B, Hoi Dick N, Lee JHS. (2013). Measurement and relationship between critical tube diameter and critical energy for direct blast initiation of gaseous detonations. *J Loss Prev Process Indust*. 26: 1293-1299.
- [17] Goodwin GB, Houim RW, Oran ES. (2016). Effect of decreasing blockage ratio on DDT in small channels with obstacles. *Combust Flame*. 173: 16-26.
- [18] Gamezo VN, Ogawa T, Oran ES. (2007). Numerical simulations of flame propagation and DDT in obstructed channels filled with hydrogen-air mixture. *Proceedings of the Combustion Institute*. 31: 2463-2471.

- [19] Kessler DA, Gamezo VN, Oran ES. (2010). Simulations of flame acceleration and deflagration-to-detonation transitions in methane-air systems. *Combust Flame*. 157: 2063-2077.
- [20] Houim RW, Ozgen A, Oran ES. (2016). The role of spontaneous waves in the deflagration-to-detonation transition in submillimetre channels. *Combustion Theory and Modelling*. 20: 1068-1087.
- [21] Zel'dovich YB, Librovich VB, Makhviladze GM. (1970). On the development of detonation in a non-uniformly pre-heated gas. *Astronautica Acta*. 15: 312-321.
- [22] Lee JH, Knystautas R, Yoshikawa N. (1978). Photochemical initiation of gaseous detonations. *Acta Astronaut*. 5: 971-982.
- [23] Gelfand BE, Khomik SV, Bartenev AM, Medvedev SP, Gronig H, Olivier H. (2000). Detonation and deflagration initiation at the focusing of shock waves in combustible gaseous mixture. *Shock Waves*. 10: 197-204.
- [24] Gray JaT, Lemke M, Reiss J, Paschereit CO, Sesterhenn J, Moeck JP. (2017). A compact shock-focusing geometry for detonation initiation: Experiments and adjoint-based variational data assimilation. *Combust Flame*. 183: 144-156.
- [25] Xiao HH, Oran ES. (2019). Shock focusing and detonation initiation at a flame front. *Combust Flame*. 203: 397-406.
- [26] Vollmer KG, Ettner F, Sattelmayer T. (2012). Deflagration-to-detonation transition in hydrogen/air mixtures with a concentration gradient. *Combust Sci Technol*. 184: 1903-1915.
- [27] Dorofeev SB, Sidorov VP, Kuznetsov MS, Matsukov ID, Alekseev VI. (2000). Effect of scale on the onset of detonations. *Shock Waves*. 10: 137-149.
- [28] Boeck LR, Kellenberger M, Rainsford G, Ciccarelli G. (2017). Simultaneous OH-PLIF and schlieren imaging of flame acceleration in an obstacle-laden channel. *Proceedings of the Combustion Institute*. 36: 2807-2814.
- [29] Boeck LR, Berger FM, Hasslberger J, Sattelmayer T. (2016). Detonation propagation in hydrogen-air mixtures with transverse concentration gradients. *Shock Waves*. 26: 181-192.
- [30] Boeck LR. (2015). Deflagration-to-detonation transition and detonation propagation in H₂-Air mixtures with transverse concentration gradients. *Technical university of munich*. 238.
- [31] Boeck LR, Hasslberger J, Sattelmayer T. (2014). Flame acceleration in hydrogen/air mixtures with concentration gradients. *Combust Sci Technol*. 186: 1650-1661.
- [32] Zheng W, Kaplan CR, Rhouim W, Oran ES. (2019). Flame acceleration and transition to detonation in methane-air mixtures with composition gradients. *Proceedings of the Combustion Institute*. 37: 3521-3528.
- [33] Karanam A, Ganju S, Chattopadhyay J. (2021). Timescale analysis, numerical simulation and validation of flame acceleration, and DDT in hydrogen-air mixtures. *Combust Sci Technol*. 193: 2217-2240.
- [34] Karanam A, Sharma PK, Ganju S. (2018). Numerical simulation and validation of flame acceleration and DDT in hydrogen air mixtures. *Int J Hydrogen Energy*. 43: 17492-17504.
- [35] Azadboni RK, Heidari A, Wen JX. (2020). Numerical studies of flame acceleration and onset of detonation in homogenous and inhomogeneous mixture. *J Loss Prev Process Indust*. 64.
- [36] Azadboni RK, Wen JX, Heidari A, Wang CJ. (2017). Numerical modeling of deflagration to detonation transition in inhomogeneous hydrogen/air mixtures. *J Loss Prev Process Indust*. 49: 722-730.

- [37] Fan J, Xiao HH. (2022). Flame acceleration and transition to detonation in non-uniform hydrogen-air mixtures in an obstructed channel with different obstacle arrangements. *Fire Saf J*. 133.
- [38] Gamezo VN, Ogawa T, Oran ES. (2008). Flame acceleration and DDT in channels with obstacles: Effect of obstacle spacing. *Combust Flame*. 155: 302-315.
- [39] Xiao H, Duan Q, Sun J. (2018). Premixed flame propagation in hydrogen explosions. *Renewable & Sustainable Energy Reviews*. 81: 1988-2001.
- [40] Xiao H, Houim RW, Oran ES. (2015). Formation and evolution of distorted tulip flames. *Combust Flame*. 162: 4084-4101.
- [41] Xiao H, Houim RW, Oran ES. (2017). Effects of pressure waves on the stability of flames propagating in tubes. *Proceedings of the Combustion Institute*. 36: 1577-1583.
- [42] Kaplan CR, Ozgen A, Oran ES. (2019). Chemical-diffusive models for flame acceleration and transition-to-detonation: genetic algorithm and optimisation procedure. *Combustion Theory and Modelling*. 23: 67-86.
- [43] Poludnenko AY, Oran ES. (2010). The interaction of high-speed turbulence with flames: Global properties and internal flame structure. *Combust Flame*. 157: 995-1011.
- [44] Ogawa T, Oran ES, Gamezo VN. (2013). Numerical study on flame acceleration and DDT in an inclined array of cylinders using an AMR technique. *Computers & Fluids*. 85: 63-70.
- [45] Liu DD, Liu ZR, Xiao HH. (2022). Flame acceleration and deflagration-to-detonation transition in narrow channels filled with stoichiometric hydrogen-air mixture. *Int J Hydrogen Energy*. 47: 11052-11067.
- [46] Xiao H, Oran ES. (2020). Flame acceleration and deflagration-to-detonation transition in hydrogen-air mixture in a channel with an array of obstacles of different shapes. *Combust Flame*. 220: 378-393.
- [47] Kessler DA, Gamezo VN, Oran ES. (2011). Multilevel detonation cell structures in methane-air mixtures. *Proceedings of the Combustion Institute*. 33: 2211-2218.
- [48] Fan J, Xiao H. (2022). Flame acceleration and transition to detonation in non-uniform hydrogen-air mixtures in an obstructed channel with different obstacle arrangements. *Fire Saf J*. 133.
- [49] Houim RW, Kuo KK. (2011). A low-dissipation and time-accurate method for compressible multi-component flow with variable specific heat ratios. *J Comput Phys*. 230: 8527-8553.
- [50] Sun M, Takayama K. (1999). Conservative smoothing on an adaptive quadrilateral grid. *J Comput Phys*. 150: 143-180.
- [51] Boeck LR, Katzy P, Hasslberger J, Kink A, Sattelmayer T. (2016). The GraVent DDT database. *Shock Waves*. 26: 683-685.
- [52] Xiao HH, Makarov D, Sun JH, Molkov V. (2012). Experimental and numerical investigation of premixed flame propagation with distorted tulip shape in a closed duct. *Combust Flame*. 159: 1523-1538.
- [53] Bychkov V, Akkerman VY, Fru G, Petchenko A, Eriksson L-E. (2007). Flame acceleration in the early stages of burning in tubes. *Combust Flame*. 150: 263-276.
- [54] Johansen CT, Ciccarelli G. (2009). Visualization of the unburned gas flow field ahead of an accelerating flame in an obstructed square channel. *Combust Flame*. 156: 405-416.